Inorganic Chemistry
ARTICLE
pubs.acs.org/IC

Loops, Chains, Sheets, and Networks from Variable Coordination of Cu(hfac)$_2$ with a Flexibly Hinged Aminoxyl Radical Ligand

Martha Baskett,[†] Armando Paduan-Filho,[‡] Nei Fernandes Oliveira, Jr.,[‡] A. Chandrasekaran,[†] Joel T. Mague,[§] and Paul M. Lahti*,[†]

[†]Department of Chemistry, University of Massachusetts, Amherst, Massachusetts 01003, United States
[‡]Instituto de Fisica, Universidade de São Paulo, Caixa Postal 66.318, 05315-970 São Paulo, Brazil
[§]Department of Chemistry, Tulane University, New Orleans, Louisiana 70118, United States

S *Supporting Information*

ABSTRACT: One pair of reactants, Cu(hfac)$_2$ = M and the hinge-flexible radical ligand 5-(3-*N*-*tert*-butyl-*N*-aminoxylphenyl)pyrimidine (**3PPN** = L), yields a diverse set of five coordination complexes: a cyclic loop M$_2$L$_2$ dimer; a 1:1 cocrystal between an M$_2$L$_2$ loop and an ML$_2$ fragment; a 1D chain of M$_2$L$_2$ loops linked by M; two 2D M$_3$L$_2$ networks of (M−L)$_n$ chains cross-linked by M with different repeat length pitches; a 3D M$_3$L$_2$ network of M$_2$L$_2$ loops cross-linking (M−L)$_n$-type chains with connectivity different from those in the 2D networks. Most of the higher dimensional complexes exhibit reversible, temperature-dependent spin-state conversion of high-temperature paramagnetic states to lower magnetic moment states having antiferromagnetic exchange within Cu−ON bonds upon cooling, with accompanying bond contraction. The 3D complex also exhibited antiferromagnetic exchange between Cu^{II} ions linked in chains through pyrimidine rings.

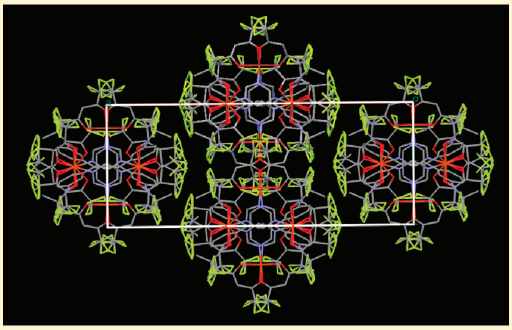

INTRODUCTION

One strategy for the design and synthesis of molecular magnetic materials is to coordinate paramagnetic transition-metal ions with organic open−shell molecules to make “hybrid” mixtures of spin sites. Nitronylnitroxides, aminoxyls, and verdazyls have all been coordinated into varying structural motifs and magnetic behaviors, combining the strong magnetic moments of transition-metal ions with diverse structural units from organic chemistry.[1] This allows many possible structural types and magnetic exchange pathways.

We have described complexation of dicationic transition-metal salts M(hfac)$_2$ = M (hfac = hexafluoroacetylacetonate) with radical ligands (L) **4PPN**[2] and **4TPN**[3] to give M$_2$L$_2$ cyclic dimers shown in Scheme 1. For higher reacting ratios of **4PPN** to M(hfac)$_2$, ML$_2$ linear triads were formed.[4] Only Co(hfac)$_2$ with **4PPN** gave an extended, 1D ribbon polymer with stoichiometry M$_3$L$_2$.[5] Higher dimensional coordination is an important goal of research to form multidimensional exchange networks in molecular magnetic materials. 1D chain systems are fairly common, 2D network systems less so, and 3D systems probably the most challenging among complexes of transition metals with radical-bearing ligands.

We tested 5-(3-[*N*-*tert*-butyl-*N*-aminoxyl]phenyl)pyrimidine (**3PPN**) as a “hinge-flexible” radical ligand and reported[6] its M$_2$L$_2$-type complexes with M(hfac)$_2$ (M = Mn, Co, Ni, Cu). The hinge flexibility was specifically designed to allow **3PPN** more conformational freedom to form extended conjugation networks than **4PPN** and **4TPN**. By varying the reaction conditions using **3PPN** and Cu(hfac)$_2$, we obtained new 1D, 2D, and 3D coordination solids, which are reported in this article.

RESULTS

3PPN was synthesized by our previous procedure[6] (Scheme 2). Unlike isomer **4PPN**,[2,7] **3PPN** decomposes upon extended storage, so it is best to store precursor **3PPNH** and make **3PPN** just before use. Fortunately, the **3PPN** solution stability was sufficient for slow crystallization of layered solutions of it with Cu(hfac)$_2$. Five new complexes shown in Table 1 were obtained: a M$_2$L$_2$·ML$_2$ 1:1 cocrystal **M3L4**, a 1D polymer **Chain**, two different 2D networks **Net2syn** and **Net2anti**, and a 3D network **Net3d**. The properties of the previously reported cyclic **M2L2** copper(II) complex[6] are also compared in the discussion below. All structures were identified by single-crystal X-ray diffraction (XRD) analyses.

M3L4 and **Chain** were only obtained in small amounts and not extensively analyzed. **Net2syn**, **Net2anti**, and **Net3d** were more readily obtained and were subjected to both room temperature and 100 K XRD crystallography, to dc magnetic susceptibility (χ vs T) studies at 1.8−300 K, and to magnetization versus field experiments (M vs H) at 0.5−1.4 K. The results are detailed in various sections below.

Received: February 21, 2011
Published: April 27, 2011

■ DISCUSSION

Design Strategy for Extending Radical Ligand Coordination Networks. In addition to the above-mentioned cyclic M_2L_2 complexes of various $M(hfac)_2$ with **4PPN**, **4PTN**, and **3PPN**, analogous structures have been reported for complexation of $Mn(hfac)_2$ and $Cu(hfac)_2$ with **4PImN**,[8,9] **3PImN**,[8,9] **4PyrN**,[9,10] and **3PyrN**[9,10] (Chart 1). Among these,[11] the only complex with possibly extended connectivity was a structurally ill-characterized product of $Mn(hfac)_2$ with **4PyrN**.[10a]

Scheme 1. Lower Dimensional Complexes of Radical Ligands 4PPN, 4TPN, and 3PPN with $Cu(hfac)_2$

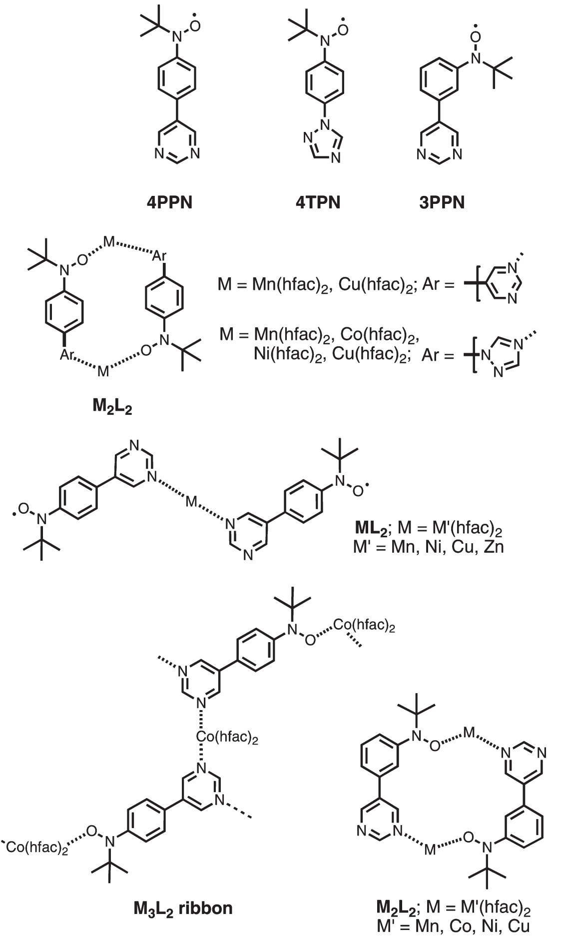

In the M_2L_2 complexes of **4PPN**[2] and **4PTN**[3] with $Mn(hfac)_2$ or $Cu(hfac)_2$, one azacycle nitrogen remained uncomplexed. Only the M_3L_2 ladder ribbon polymer[5] from $Co(hfac)_2$ and **4PPN** showed extended coordination. A possible hindrance to forming extended networks from **4PPN** and **4PTN** is their limited conformational variability. **3PPN** can accommodate both linear and sharply bent extensions across the pyrimidine unit through anti *and* syn aminoxyl conformers (Scheme 3). **3PPN** is hinged to accommodate planar chain extension, tight helical chain extension, and loop formation, among other possibilities. Yamada et al. have explicitly noted the structural richness possible in magnetic complexes with hinged ligands.[12]

The structural diversity of Table 1 products shows how the hinged radical ligand **3PNN** provided more possibilities for complexation by comparison to isomer **4PNN**. This causes complications because product formation was sensitive to $Cu(hfac)_2$/**3PPN** reactant ratios and to the solvent types and amounts. Sometimes it was necessary to remove coprecipitated $Cu(hfac)_2$ manually from the desired product. Multiple phases occasionally cocrystallized from a reaction mixture but could be manually separated based on their different appearances. The use of XRD was important to check the unit cell parameters of different batches of product and establish identity.

Although no systematic effort was made to determine the mechanisms of product formation, a tentative proposal is given in Scheme 4, based on the structural features found in the Table 1 complexes. An initially formed MLN intermediate could azacomplex to another **3PPN** to give ML_2 intermediates. Neither linear nor bent ML_2 complexes were isolated for L = **3PPN**, but both structures are part of the complexes in Table 1. M_2L_2 systems[5] could form by condensing two MLN or MLO intermediates [presumably azaphilic Cu(II) favors MLN]. All processes are shown as equilibria because recrystallizing initially isolated products occasionally yielded other complexes.

$Cu_2(3PPN)_2(hfac)_4 \cdot Cu(3PPN)_2(hfac)_2$ (M3L4). This cluster is a 1:1 cocrystal of a Cu_2(**3PPN**)$_2(hfac)_4$ M_2L_2 loop with a Cu(**3PPN**)$_2(hfac)_2$ = ML_2 fragment. Although the ML_2 fragment was never isolated alone, its incorporation into **M3L4** suggests that it and M_2L_2 are simultaneously present in significant amounts during crystallization, consistent with Scheme 4.

Figure 1 shows a structure diagram of **M3L4** (ORTEP[13] diagrams are given in the Supporting Information). Table 2

Scheme 2. Synthesis of 3PPN

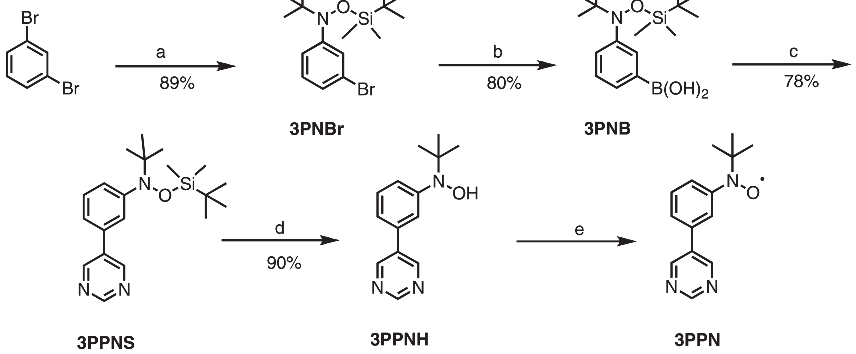

Table 1. Complexes of $Cu(hfac)_2$ with 3PPN [$M = Cu(hfac)_2$]

Table 1. Complexes of $Cu(hfac)_2$ with **3PPN**. $M = Cu(hfac)_2$.

Designation	Stoichiometry	Structure ($M = Cu(hfac)_2$)
M3L4	$Cu_3(3PPN)_4(hfac)_6$ (Olive-green blocks)	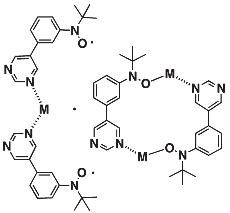
M2L2	$Cu_2(3PPN)_2(hfac)_4$ (Greenish-brown blades)	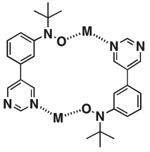
Chain	$Cu_3(3PPN)_2(hfac)_6$ (Light green needles)	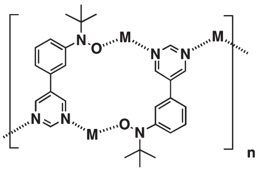
Net2syn	$Cu_3(3PPN)_2(hfac)_6$ (Emerald blocks)	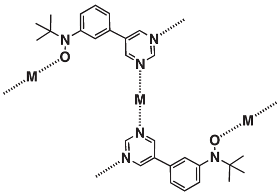
Net2anti	$Cu_3(3PPN)_2(hfac)_6$ (Yellow-green plates)	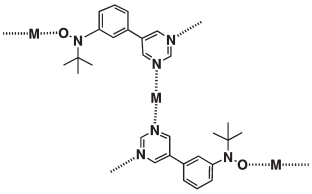
Net3d	$Cu_3(3PPN)_2(hfac)_6$ (Green-black prisms)	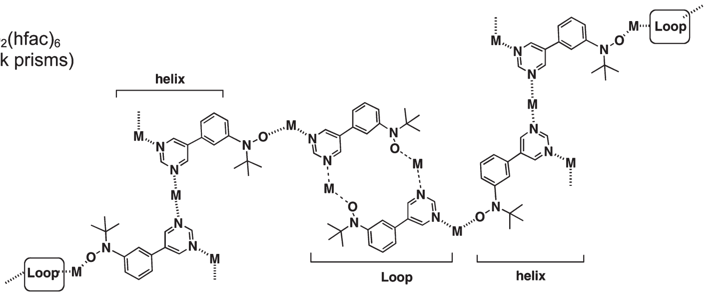

summarizes its XRD parameters; Figure 2 focuses on its copper(II) ligand spheres. At all points in this article, "Cu−ON" will refer to a copper−aminoxyl bond involving the aminoxyl oxygen. The ML_2 fragment has a somewhat distorted octahedral copper(II) coordination, with **3PPN** units in the "bent" ML_2 geometry of Scheme 4. The M_2L_2 loop is centrosymmetric, having both **3PPN** units in the *syn*-aminoxyl conformations required to form a loop. The Cu1−O5N bond is fairly short and thus equatorial. The equatorial pyrimidine Cu1−N1 bond in the loop is shorter than the Cu2−N31 or Cu2−N34 bonds in the ML_2 unit. The ML_2 and M_2L_2 fragments are associated in the **M3L4** cocrystal by favorable interaction of the C55−H bond of a ML_2 unit with the otherwise uncoordinated pyrimidine N2 of an M_2L_2 unit (Figure 1); $r(C55\cdots N2) = 3.621(7)$ Å. A riding model estimate of the hydrogen atom on C55 puts it about 2.7 Å from N2. Although the small isolated amount of **M3L4** precluded magnetic measurements, the short Cu−ON bond lengths in its M_2L_2 loops are comparable to those for aminoxyls that are equatorially complexed to Cu^{II} and exhibit antiferromagnetic (AFM) Cu−ON exchange,[14] including the low-temperature form of **M2L2** discussed below.

$Cu_2(3PPN)_2(hfac)_4$ (M2L2). We reported formation of the M_2L_2 complex of $Cu(hfac)_2$ with **3PPN** previously.[6] Figure 3 shows its structure, and Table 2 gives crystallographic details. **M2L2** is structurally similar to the loops in **M3L4** and (as we shall see) **Chain** and **Net3d**. **M2L2** has two distinct forms in the lattice that exhibit reversible coordination sphere changes with the temperature (Figure 4). At room temperature, both forms have much longer Cu—ON bond lengths than the analogous loop fragments of **M3L4** and **Net3d**. Cooling to 100 K causes the axial Cu—ON bonds to contract and change to equatorial, with corresponding color changes from brownish at room temperature to green at low temperatures. As we shall see, most of the network complexes of Table 1 also exhibit temperature-dependent Cu—ON bond length changes with their magnetism. **M2L2** is thus a model for behavior in the more complex structures.

Both χ and χT vs T plots for **M2L2** steadily decrease from room temperature to minima at about 100 K, as shown in Figure 5. If all four possible spins in **M2L2** were independent, χT at high temperatures would plateau at ~1.5 emu·K/Oe·mol; for ferromagnetic (FM) exchange in the Cu—ON bonds, the plateau would be at ~2.0 emu·K/Oe·mol. The room temperature χT is only about half the free-spin value, with no plateau in the upper temperature region. So, at least half of the **M2L2** lattice already has some Cu—ON AFM spin pairing at room temperature, presumably form B in Figure 4 with its shorter Cu—ON bonds. At lower temperature, both forms of **M2L2** lose the paramagnetic moment with Cu—ON bond contraction. The magnetization versus field data for **M2L2** show much less than one spin per mole of **M2L2** (consistent with the χ and χT results). We used a 10 000 Oe field to increase the signal for the susceptibility measurements; the magnetization versus field dependence is still linear in this range at 1.25 K, so the Figure 5 data are still in the weak-field regime.

Whether the spins in the **M2L2** complex are nearly independent or FM-coupled at higher temperatures, the decreases in χ and χT with the temperature are hallmarks of spin-state conversion[15] to a low-spin state. The transition occurs over a fairly broad temperature range rather than a sudden, synergistic change of molecules in all lattice sites. The conversion from a paramagnetic state with longer Cu—ON bond lengths to low-spin AFM exchange at shorter bond lengths is attributable to changes in the overlap between the magnetic orbitals of octahedral copper(II) and aminoxyl: details have been given elsewhere.[1f,6,16] In principle, the magnetic changes could be due simply to thermal depopulation of paramagnetic excited states in the Cu—ON bonds, but we feel that correlation of the geometry changes with the color and magnetic changes supports spin-state conversion.

Complex $[Cu_3(3PPN)_2(hfac)_6]_n$ (Chain). The **Chain** complex structure is shown in Figure 6; crystallographic details are given in Table 1. **Chain** incorporates M_2L_2 loops linked by $Cu(hfac)_2$ to form 1D chains, such that its **3PNN** units are fully coordinated to give stoichiometry M_3L_2. Its M_2L_2 loops are structurally similar to those in **M3L4** and **M2L2**, with somewhat distorted octahedral Cu1 ligand spheres. The loop Cu1—O7N bonds are intermediate in length among those in this study (Figure 7, 1.99 Å).

The chain link Cu2—N3 bonds in **Chain** are significantly longer than the Cu1—N bonds of the loop unit or those in the analogous ML_2 fragment of **M3L4**: r(Cu2—N3) = 2.27 Å (Figure 7) versus 2.03—2.04 Å (Figure 4) in **M3L4**. The chain

Chart 1

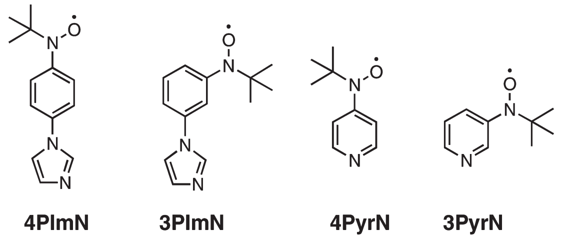

Scheme 3. Complexation Geometries Accommodated by 4PPN and 3PPN

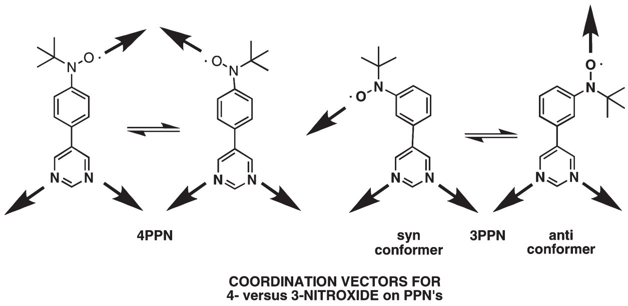

Scheme 4. Tentative Mechanistic Scheme for 3PPN Complexation[a]

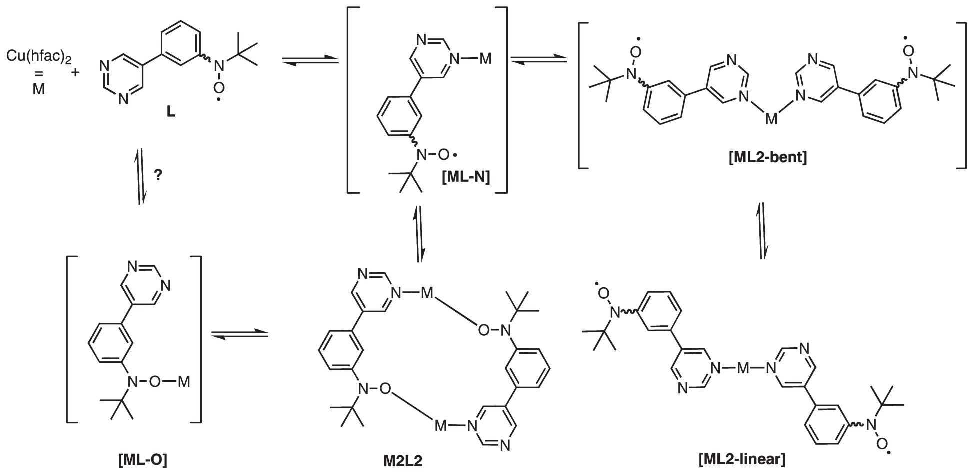

[a] Bracketed structures are putative.

link is bent with ∠N3−Cu2−N(3_2) = 82.9°. The Cu2−O5(hfac) bonds are contracted and short in the ML_2 unit of **Chain**, whereas the analogous Cu−O(hfac) bonds are long and axial in the ML_2 unit of **M3L4**.

The chains of **Chain** pack along the crystallographic *c* axis with contact between the hfac CF_3 groups on the periphery of each chain axis, at an interchain distance of 17.5 Å, which should limit **3PPN** and Cu(II) spins to intrachain exchange. Views of the chain packing are given in the Supporting Information. Unfortunately, insufficient **Chain** was obtained for reliable magnetic analysis. However, its short Cu−ON bond lengths are similar to those of M_2L_2 form B at 100 K (compare Figures 4 and 7). As we shall see below, coordinating Cu_2L_2 loops into larger network solids seems to encourage bond shortening in Cu−ON of the loops.

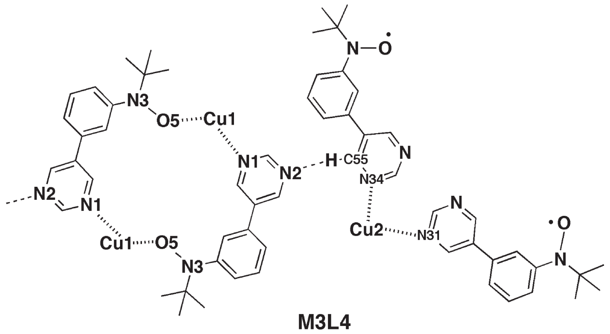

M3L4

Figure 1. Structure diagram of the 1:1 cocrystal molecular complex **M3L4**.

2D Sheet Complex $[Cu_3(3PPN)_2(hfac)_6]_n$ (Net2syn). The 2D sheet complexes **Net2syn** and **Net2anti** have the same bond connectivity but different secondary structure and magnetic properties. In both, $(Cu\cdots PyrimPhNO\cdots)_n$ chains leave a pyrimidine nitrogen atom of each **3PPN** for $Cu(hfac)_2$ cross-linking to a nearby chain. However, their chain geometries are quite different.

The structure of **Net2syn** is shown in Figures 8 and 9, and its crystallographic parameters are given in Table 3. Its $(Cu\cdots PyrimPhNO\cdots)_n$ chains are helices wherein **3PPN** units have a *syn*-aminoxyl to pyrimidine relationship, similar to **3PPN** in the M_2L_2 loop units of **M3L4**, **M2L2**, and **Chain**. If one imagines twisting an M_2L_2-type loop at a Cu−ON bond to form an "S"-shape, that would give the helical repeat unit of the **Net2syn** chains. Within the chains, the Cu1−O7N bond length is 1.97 Å (Figure 9), and the O4−Cu1−O1(hfac) bonds are the longest,

Table 2. Crystallographic Data for Molecular and 1D Chain Complexes of $Cu(hfac)_2$ with 3PPN

	M3L4	M2L2	Chain
chemical formula	$C_{124}H_{104}Cu_4F_{48}N_{18}O_{22}$	$C_{48}H_{36}Cu_2F_{24}N_6O_{10}$	$C_{58}H_{38}Cu_3F_{36}N_6O_{14}$
fw	3364.41	1439.91	1917.6
temperature (K)	293	298 [100]	298
space group	triclinic, $P\bar{1}$	triclinic, $P\bar{1}$	monoclinic, $C2/c$
a (Å)	11.4071(1)	9.6621(2) [9.44230(10)]	32.9455(4)
b (Å)	18.0922(2)	16.0241(3) [15.7864(2)]	11.4448(2)
c (Å)	19.2627(3)	19.6090(5) [19.5298(4)]	23.3160(3)
α (deg)	77.4891(4)	76.5851(8) [76.6127(6)]	90.0
β (deg)	80.8945(4)	81.6545(8) [81.7446(6)]	119.7464(7)
γ (deg)	79.3408(7)	82.4981(17) [81.6369(8)]	90.0
V (Å^3)	3785.01(8)	2907.04(11) [2769.31(7)]	7632.96(19)
Z	1	2 [2]	4
cryst dimens (mm^3)	0.50 × 0.50 × 0.20	1.00 × 0.75 × 0.10	1.00 × 0.50 × 0.50
D_{calc} (Mg/m^3)	1.476	1.868	1.669
θ range (deg)	4.10−25.08	4.08−25.09	4.09−25.01
$F(000)$	1698	1440	3804
μ (mm^{-1})	0.561	0.978 [0.991]	0.978
data collection method	$\omega-2\theta$ scans	$\omega-2\theta$ scans	$\omega-2\theta$ scans
collected/unique reflns	7823/3982	16 661/10 141 [9714/7671]	12 452/6642
criterion obsd reflns	$I > 2\sigma(I)$	$I > 2\sigma(I)$	$I > 2\sigma(I)$
R_{int}	0.0208	0.0266 [0.0361]	0.0221
ranges of h, k, l	$-12 \rightarrow h \rightarrow +13$	$-11 \rightarrow h \rightarrow +11$ $[-11 \rightarrow h \rightarrow +10]$	$-38 \rightarrow h \rightarrow +39$
	$-21 \rightarrow k \rightarrow +121$	$-19 \rightarrow k \rightarrow +19$ $[-18 \rightarrow k \rightarrow +18]$	$-12 \rightarrow k \rightarrow +13$
	$-22 \rightarrow l \rightarrow +21$	$-23 \rightarrow l \rightarrow +21$ $[-22 \rightarrow l \rightarrow +22]$	$-27 \rightarrow l \rightarrow +27$
completeness to 2θ	0.985	0.978 [0.986]	0.985
no. of reflns	13 265	10 202 [9714]	6642
no. of restraints	828	0 [0]	0
no. of param	970	799 [799]	552
GOF on F^2	1.034	1.026 [1.029]	1.028
$\Delta\rho_{max}$, $\Delta\rho_{min}$ (e/Å^3)	0.943, −0.540	0.930, −0.852 [1.053, −0.977]	0.905, −0.569
R1, wR2 [$I > 2\sigma(I)$]	0.0753, 0.2102	0.0798, 0.2001 [0.0522, 0.1234]	0.0869, 0.2362
R1, wR2 (all)	0.0953, 0.2284	0.1029, 0.2189 [0.0702, 0.1336]	0.1074, 0.2590

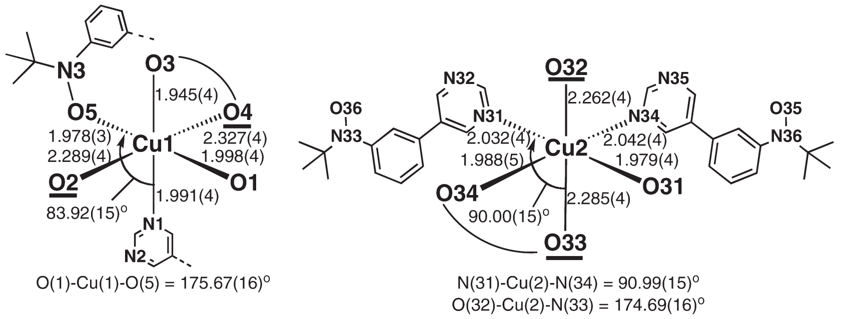

Figure 2. Coordination sphere bonding for **M3L4**. Bond lengths are in angstroms and angles in degrees. Long bond ligation sites are underlined.

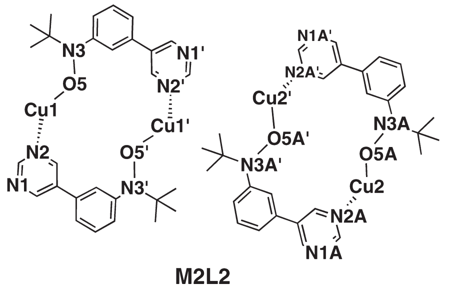

Figure 3. Structure diagram for the M_2L_2 molecular complex of $Cu(hfac)_2$ with **3PPN**.

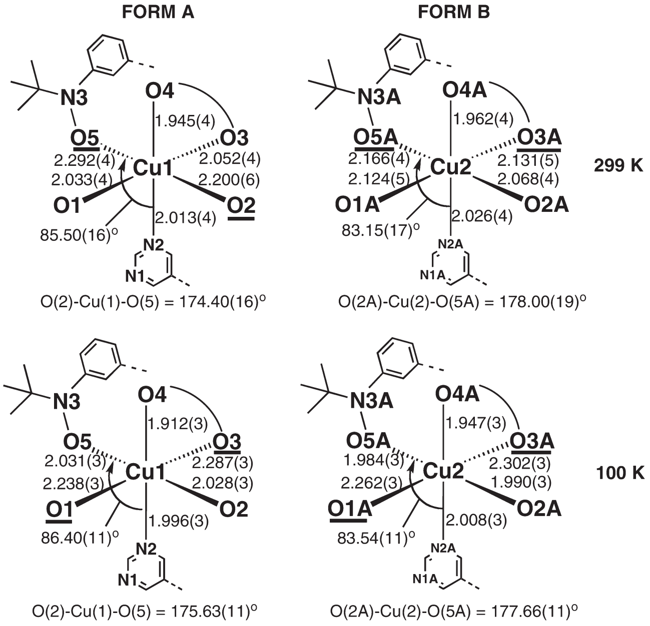

Figure 4. Ligand-sphere bonding parameters for **M2L2** at 299 and 100 K. Bond lengths are in angstroms and angles in degrees. Long bond ligation sites are underlined.

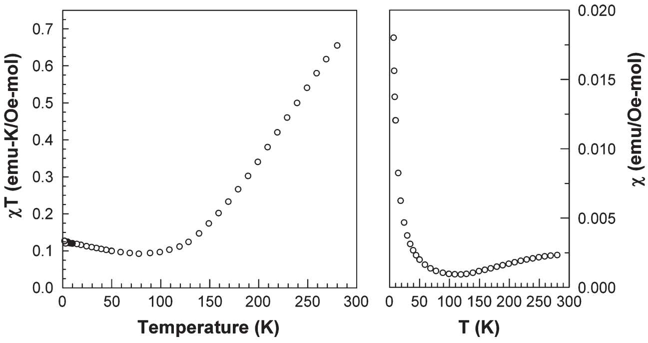

Figure 5. χT (left) and χ (right) vs T plots for the M_2L_2 complex at 10 000 Oe.

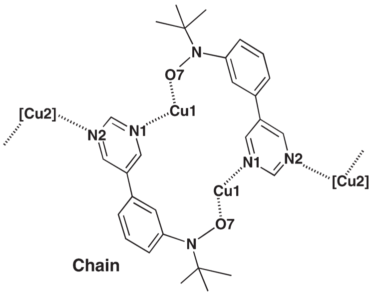

Figure 6. Structure diagram for 1D polymer complex **Chain**.

although bent from an ideal trans diaxial angle with ∠O−Cu−O = 169°. The Cu1−N1 pyrimidine bond length along the chains is 2.03 Å, similar to that in the previously discussed M_2L_2 loop units.

Neighboring helices propagate in alternating directions, cross-linked across pyrimidine nitrogen atoms of **3PPN** by Cu2 to form 2D networks. The Cu2−N3 cross-links of 2.48 Å are much longer than the intrahelix Cu1−N1 bonds and, therefore, axial. The hfac oxygen atoms in the Cu2 coordination sphere are equatorial with short lengths (Figure 9). Upon cooling of single crystals to 100 K, the helix repeat distance decreases somewhat from 12.1 to 11.7 Å, but the ligand spheres of Cu1 and Cu2 do not change much. The 2D networks in **Net2syn** stack as roughly planar slabs, with interslab contacts between the hfac CF_3 groups on the peripheries above and below, as shown in Scheme 5 (with details in the Supporting Information).

The magnetic susceptibility of **Net2syn** shows essentially Curie−Weiss behavior from room temperature to 1.8 K (Figure 10), with C = 1.04 emu·K/Oe·mol and θ = (−)0.5 K. The χT data have a high temperature plateau of ~1.0 emu·K/Oe·mol down to about 15 K. The decrease in χT at lower temperatures indicates only weak AFM exchange interactions between spin sites, consistent with the small Weiss constant.

Magnetization versus field studies at 0.5 K show a step at ~1 μ_B/mol (20 000 Oe) and then an increase to a bit above

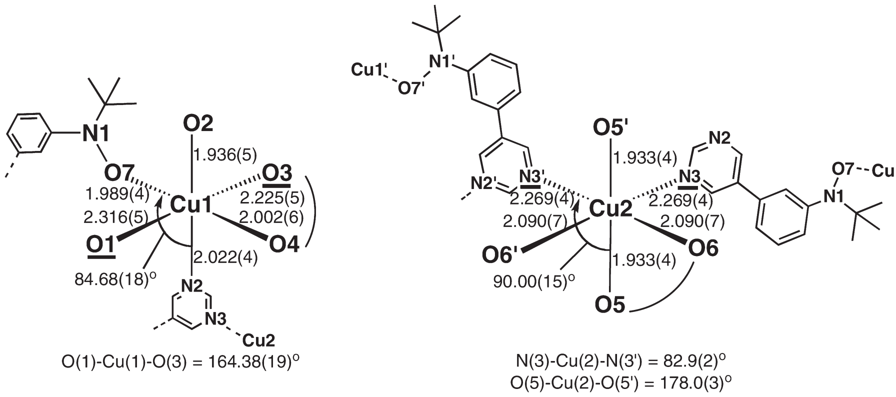

Figure 7. Ligand-sphere bonding parameters for **Chain** at room temperature. Bond lengths are in angstroms and angles in degrees. Long bond ligation sites are underlined.

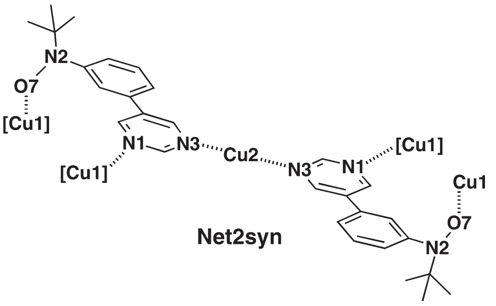

Figure 8. Structure diagram for 2D network complex **Net2syn**.

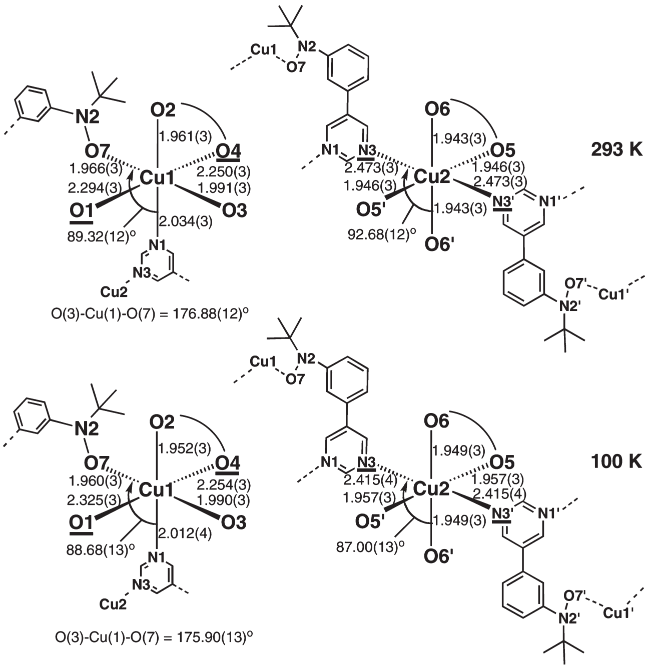

Figure 9. Ligand-sphere bonding parameters for **Net2syn** at 293 and 100 K. Bond lengths are in angstroms and angles in degrees. Long bond ligated atoms are underlined.

Table 3. Crystallographic Parameters for 2D Complex Net2syn

temperature (K)	298	100
chemical formula	$C_{58}H_{38}Cu_3F_{36}N_6O_{14}$	$C_{58}H_{38}Cu_3F_{36}N_6O_{14}$
fw	1917.56	1917.56
cell setting, space group	monoclinic, $P2_1/n$	monoclinic, $P2_1/n$
a (Å)	15.1227(2)	14.9104(2)
b (Å)	12.0542(1)	11.68780(10)
c (Å)	20.8771(3)	20.5148(2)
α (deg)	90.	90.
β (deg)	93.1804(5)	92.6405(5)
γ (deg)	90.	90.
V (Å^3)	3799.87(8)	3571.31(7)
Z	2	2
D_{calc} (g/cm^3)	1.676	1.783
θ range (deg)	4.11−25.13	4.18−25.03
F(000)	1902	1902
μ (mm^{-1})	0.982	1.045
data collection method	$\omega-2\theta$ scans	$\omega-2\theta$ scans
collected/unique reflns	12 445/6646	10 546/6208
criterion for obsd reflns	$I > 2\sigma(I)$	$I > 2\sigma(I)$
R_{int}	0.0211	0.0241
ranges of h, k, l	$-17 \rightarrow h \rightarrow +17$	$-17 \rightarrow h \rightarrow +17$
	$-14 \rightarrow k \rightarrow +12$	$-12 \rightarrow k \rightarrow +13$
	$-24 \rightarrow l \rightarrow +24$	$-24 \rightarrow l \rightarrow +24$
completeness to 2θ	0.981	0.998
reflns/restraints/param	6646/0/529	6208/0/529
GOF on F^2	1.030	1.144
$\Delta\rho_{max}$, $\Delta\rho_{min}$ (e/Å^3)	0.717, −0.482	1.820, −0.914
R1, wR2 [$I > 2\sigma(I)$]	0.0562, 0.1474	0.0499, 0.1390
R1, wR2 (all)	0.0751, 0.1665	0.0561, 0.1422

2 μ_B/mol at 50 000 Oe and above. These results indicate at least two distinct spin carriers. The short Cu−ON bonds in **Net2syn** seemed consistent with AFM pairing of Cu1 and aminoxyl spins,[14] leaving the cross-linker Cu2 ions as the main source of the magnetic moment at low temperature. To probe the possibility that **Net2syn** was significantly contaminated with other products of the reaction between Cu(hfac)$_2$ and **3PPN**, bulk powder XRD studies were carried out at room temperature. The experimental wide-angle X-ray scattering pattern is a good match for that expected from the single-crystal XRD of **Net2syn**

Scheme 5. Schematic Representation of a 2D Slab in Net2syn (above, View of One Slab from above) and Interslab Packing (below, Edge-On View)[a]

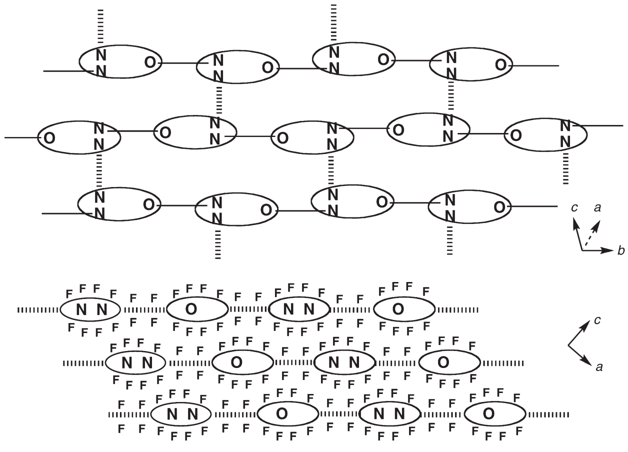

[a] Pyrimidine nitrogen (NN) and aminoxyl oxygen (O) atoms are shown to indicate alignment of the **3PPN** units. Helical chains propagate along solid bonds; cross links are dashed bonds. The lower figure shows interslab packing, with fluorine-rich regions shown by F.

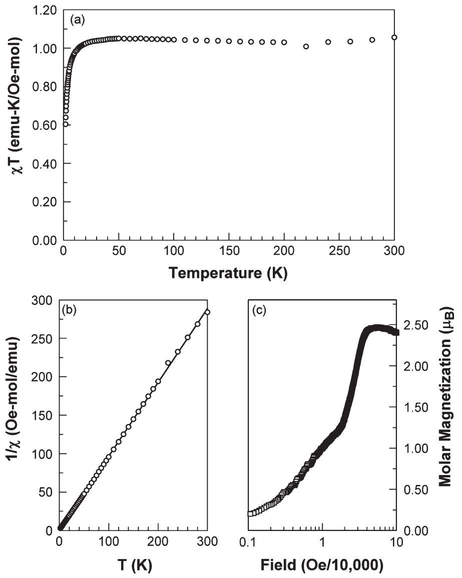

Figure 10. Paramagnetic susceptibility and magnetization data for **Net2syn**. Plot a shows χT data vs T, and plot b shows $1/\chi$ vs T, both obtained at 100 Oe external field. The solid line in plot b is the Curie−Weiss fit to data <50 K. Plot c shows the magnetization versus field data at 0.54 K.

(Supporting Information). **Net2syn** in the bulk seems to be all or almost only the structure found by multiple single-crystal XRD analyses in this study. As described in the following section, both structure and magnetism are quite different in the allotropic **Net2anti** samples.

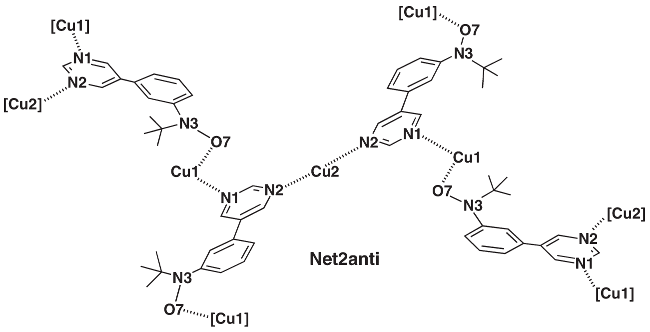

Figure 11. Structure diagram for 2D network complex **Net2anti** at room temperature.

Scheme 6. Schematic of 2D Corrugated Sheet in Net2anti (above, View of One Slab from above) and Sheet Packing (below, Edge-On View)[a]

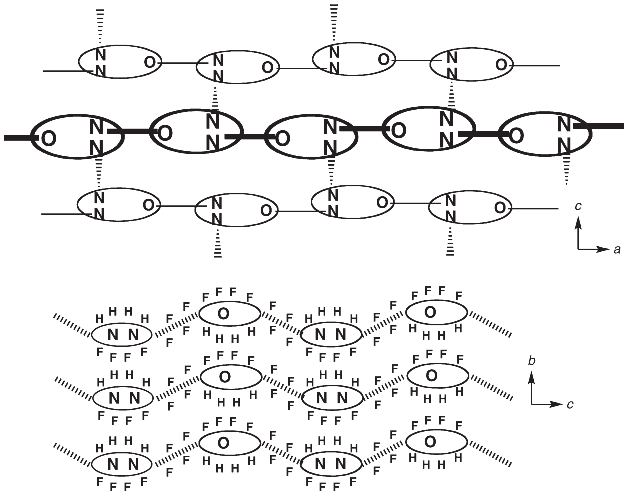

[a] In the upper view, pyrimidine nitrogen (NN) and aminoxyl oxygen (O) atoms are shown to indicate alignment of the **3PPN** units. Zigzag chains propagate along the solid bonds; cross-links are dashed bonds. The lower figure shows interslab packing, with fluorine-rich regions F and hydrogen-rich regions H.

2D Sheet Complex $[Cu_3(3PPN)_2(hfac)_6]_n$ (Net2anti). As mentioned above, **Net2anti** and **Net2syn** have the same connectivity but different coordination geometries and radical ligand conformation. Figure 11 shows the **Net2anti** structure, in which the $(Cu\cdots\mathbf{3PNN}\cdots)_n$ chains have all hfac ligands syn on one side and all **3PPN** groups syn on the opposite side, giving zigzag chains with a repeat length of 19.6 Å at room temperature. **Net2syn** has hfac and **3PPN** groups on *alternating* sides of its chains, and its 12.1 Å helix repeat distance is much shorter. In **Net2anti**, the aminoxyl groups are anti to the **3PPN** pyrimidine group (not syn, as in **Net2syn** and other complexes discussed to this point). However, **Net2anti** interchain **3PPN**−Cu2−**3PPN** cross-links are quite similar to those in **Net2syn**. Overall, the **Net2anti** networks look like corrugated sheets rather than the planar slabs of **Net2syn**. The sheets in **Net2anti** form close contacts between hfac CF_3 groups on the convex faces of the sheet and phenyl CH groups of the **3PPN** units in the concave faces, as shown in Scheme 6 (see also the Supporting Information). With all hfac units on one side of each chain, rather than spiraling around as in the helices of **Net2syn**, the plane-to-plane intersheet distance in **Net2anti** is only 8.7 Å at room temperature, much less than that in **Net2syn**.

Table 4. Crystallographic Parameters for 2D Complex Net2anti

temperature (K)	298	173	100
chemical formula	$C_{58}H_{38}Cu_3F_{36}N_6O_{14}$	$C_{58}H_{38}Cu_3F_{36}N_6O_{14}$	$C_{58}H_{38}Cu_3F_{36}N_6O_{14}$
fw	1917.56	1917.56	1917.56
cell setting, space group	orthorhombic, *Pbca*	monoclinic, $P2_1/c$	monoclinic, $P2_1/c$
a (Å)	19.6467(13)	16.545(3)	16.402(2)
b (Å)	17.4889(12)	22.703(3)	22.618(3)
c (Å)	22.7491(6)	19.720(3)	9.711(2)
α (deg)	90.0	90.0	90.0
β (deg)	90.0	94.231(2)	92.438(2)
γ (deg)	90.0	90.0	90.0
V (Å^3)	7834.71(16)	7387.2(19)	7290(1)
Z	4	4	4
D_{calc} (g/cm^3)	1.634	1.724	1.747
θ range (deg)	2.07−26.44	2.07−26.41	1.25−27.14
F(000)	3804	3804	3804
μ (mm^{-1})	0.957	1.010	1.024
data collection method	$\omega-2\theta$ scans	$\omega-2\theta$ scans	$\omega-2\theta$ scans
collected/unique reflns	116 959/8015	156 975/157 398	82 396/82 115
criterion for obsd reflns	$I > 2\sigma(I)$	$I > 2\sigma(I)$	$I > 2\sigma(I)$
R_{int}	0.0687	0.000	
ranges of h, k, l	$-24 \rightarrow h \rightarrow +24$ $-21 \rightarrow k \rightarrow +21$ $-28 \rightarrow l \rightarrow +28$	$-20 \rightarrow h \rightarrow +20$ $-28 \rightarrow k \rightarrow +28$ $-24 \rightarrow l \rightarrow +24$	$-20 \rightarrow h \rightarrow +21$ $-29 \rightarrow k \rightarrow +29$ $-25 \rightarrow l \rightarrow +25$
reflns/restraints/param	8015/74/574	157 398/0/1064	82 396/0/1064
GOF on F^2	1.041	0.756	0.883
$\Delta\rho_{max}$, $\Delta\rho_{min}$ (e/Å^3)	0.617, −0.368	1.653, −0.633	1.820, −0.914
R1, wR2 [$I > 2\sigma(I)$]	0.0759, 0.2445	0.0541, 0.0913	0.0540, 0.0948
R1, wR2 (all)	0.1348, 0.3115	0.1385, 0.1086	0.1060,0.1078

Net2anti has an orthorhombic *Pbca* space group at room temperature, but upon cooling, it undergoes twinning with a phase change to monoclinic $P2_1/c$ (see Table 4). The twinned structure units are quite similar (Figure 12 and Supporting Information) and readily revert to the *Pbca* phase upon rewarming. Other examples of reversible phase changes with transformation from higher to lower crystallographic symmetry accompanied by nonmerohedral twinning have been reported.[17] The bulk phase change in **Net2anti** correlates with changes in the Cu1−ON ligand sphere (Figure 12). At room temperature, the Cu1−ON bond and trans-related Cu−O(hfac) bond are long and axial. Cooling to 100 K shortens both bonds: two other trans-related Cu−O(hfac) bonds lengthen to become new axial substituents.

The χT vs T plot for **Net2anti** (Figure 13) decreases from ∼0.6 emu·K/Oe·mol at room temperature to a minimum of 0.4 emu·K/Oe·mol at 200 K. Curie−Weiss analysis from the $1/\chi$ vs T plot yields $C = 0.489$ emu·K/Oe·mol, where $T < 50$ K, with $\theta = (+)0.3$ K. The Curie constant corresponds to one $S = {}^1/_2$ per mole unit with $g_{\mathrm{eff}} = 2.28$. The magnetization versus field data at 0.55 K show fairly rapid saturation at 1.07 μ_B, consistent with one $S = {}^1/_2$ per mole unit, presumably from the Cu2 ions alone. The lack of magnetic contribution from the Cu1−ON bond at lower temperature occurs as a result of loss of the spin moment upon cooling (attributed to spin-state conversion due to bond shortening).

3D Network Complex $[Cu_3(3PPN)_2(hfac)_6]_n$ (Net3d). Complex **Net3d** is structurally the most intricate of the Table 1 complexes, incorporating chains and loops into a highly cross-linked 3D network, with multiple types of Cu−ON and Cu−pyrimidine coordination. Unlike the behavior in the 2D networks, the aminoxyl groups in **Net3d** do not participate in chain formation but instead only form loops and cross-links. Instead, **Net3d** chains come from alternating bent and linear Pyrim−Cu−Pyrim connections in 1D $(\mathrm{Cu}\cdots\mathrm{pyrimidine})_n$ chains. Table 5 gives its crystallographic parameters; Figure 14 shows a simplified schematic of the connectivities and **3PNN** conformations in **Net3d** and the 3D connection of loops and chains. The 3D lattice has ellipsoidal void channels of about 9 Å (a axis) by 16 Å (b axis) along the crystallographic c axis (Figure 15). Hexane solvent incorporation in these may help template the surprisingly ready formation of **Net3d**.

The $(\mathrm{Cu}\cdots\mathrm{pyrimidine})_n$ chains have pendant phenylaminoxyl groups (part of **3PPN** molecules) with aminoxyls anti to the pyrimidine (Figure 14) and radiating around the chain. The chain repeat length is about 14 Å long. These chain-pendant aminoxyls cross-link through relatively long [r(Cu1−O1[N]) = 2.195(4) Å] bonds to M_2L_2 loop units (red and yellow in Figure 14) to other chains. The M_2L_2 loops of **Net3d** are

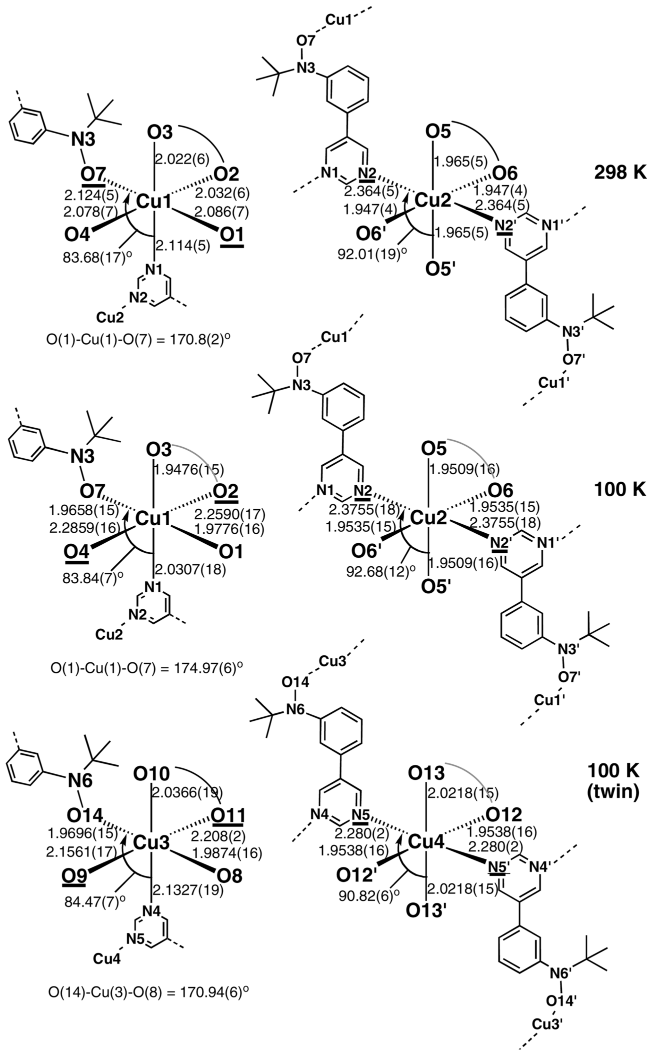

Figure 12. Ligand-sphere bonding parameters for **Net2anti**. Bond lengths are in angstroms and angles in degrees. Long bond ligated atoms are underlined.

structurally similar to loops in **M3L4** and **Chain**, having short Cu−ON bonds to the syn conformer aminoxyl groups.

Like **M2L2** and **Net2anti**, **Net3d** undergoes temperature-dependent geometry changes (Figure 16). The **Net3d** loops already have short Cu−ON bonds at room temperature that shorten only by 0.01 Å upon cooling to 100 K. However, the chain-to-loop Cu1−O1N cross-links shorten by 0.2 Å when cooled, changing from axial to equatorial; this is the presumed main source of the magnetic spin-state conversion described below.

Like **Net2anti**, **Net3d** shows a decrease in χT upon cooling (Figure 17), but more gradually from ~0.5 emu·K/Oe·mol at 300 K to ~0.38 emu·K/Oe·mol over the range 150−80 K, then a drop again to a minimum of 0.2 emu·K/Oe·mol at 7 K, and then a small increase to 2 K. The $1/\chi$ vs T plot of Figure 17 can be divided into two main regions: $T > 150$ K, with Curie constant $C = 1.44$ emu·K/Oe·mol and a very large $\theta = (-)400$ K; $T < 100$ K, with $C = 0.366$ emu·K/Oe·mol and $\theta = (-)5.2$ K.

The higher temperature Curie constant is consistent with one $S = 1$ unit plus one $S = {}^1/_2$ unit with $g_{avg} \sim 2.05$ for both. The short Cu2−O2N bonds in the M_2L_2 loops of the structure (Figure 16) suggest that their spins are already AFM-paired, with no paramagnetic contribution. However, the long Cu1−O1N bonds at room temperature in the cross-links are consistent with independent spins or FM exchange; these could contribute an $S = 1$ unit to the susceptibility at higher temperature, with Cu(II) ions in the (Cu−pyrimidine)$_n$ chains contributing $S = {}^1/_2$.

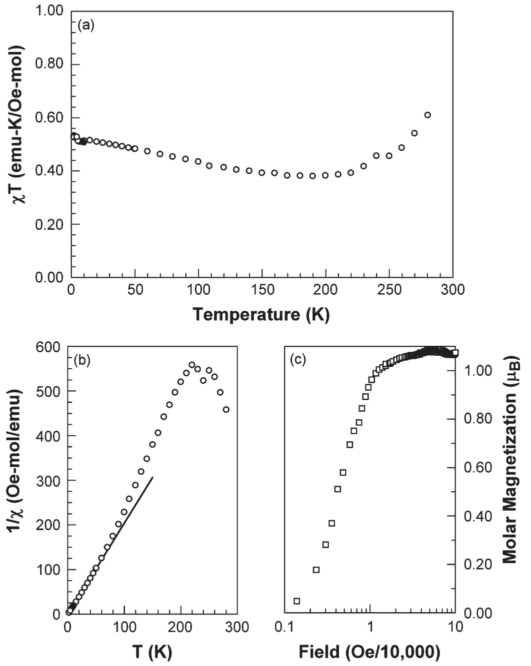

Figure 13. Paramagnetic susceptibility and magnetization data for **Net2anti**. Plot a shows χT data vs T, and plot b shows $1/\chi$ vs T both obtained at 500 Oe external field. The solid line in plot b is the Curie−Weiss fit to data <50 K. Plot c shows magnetization versus field data at 0.55 K.

The large negative Weiss constant of the Curie plot data above 150 K is attributed to spin conversion of the Cu1−O1N cross-links, with AFM exchange induced upon cooling. Below 100 K, the Cu1−O1N units are fully spin-paired, leaving only the Cu^{II} ions of the chains magnetically active: their $S = {}^1/_2$ contribution is in good agreement with the Curie constant in this region. Magnetization versus field measurements at 1.4 K for **Net3d** saturate at about 1 μ_B (Figure 17), also consistent with only the $S = {}^1/_2$ spin Cu^{II} ions of the chains remaining magnetically active at this temperature.

The further decrease in χT of **Net3d** below 50 K and the negative Weiss constant for a $T < 100$ K Curie plot indicate an additional AFM exchange interaction. Only the Cu3 and Cu4 ions in the (Cu−pyrimidine)$_n$ chains should be magnetically active at this temperature, meta-linked through pyrimidine rings of the **3PPN**. *m*-Phenylene-type units typically are FM exchange linkers save for cases of significant geometric or heteroatom substituent perturbation.[18] However, both FM and AFM exchange are reported for paramagnetic metal cations linked through pyrimidine; a summary with leading references is given by Glaser et al.[19] Computational studies by Mohri et al.[20] indicate that a cross-ring σ-overlap interaction favors AFM exchange (Scheme 7), consistent with the AFM downturn below 50 K in **Net3d**. This is unique among the Table 1 complexes because only **Net3d** forms extended [Cu^{II}−pyrimidine]$_n$ chains. Interaction between Cu^{II} ions is unlikely to involve spin polarization of the pyrimidine ring caused by the

Table 5. Crystallographic Parameters for 3D Complex Net3d

temperature (K)	298	173	100
chemical formula	$C_{58}H_{38}Cu_3F_{36}N_6O_{14}$	$C_{58}H_{38}Cu_3F_{36}N_6O_{14}$	$C_{58}H_{38}Cu_3F_{36}N_6O_{14}\cdot{}^1/_2C_6H_{14}$
fw	1917.56	1917.56	1960.65
cell setting, space group	monoclinic, $C2/c$	monoclinic, $C2/c$	monoclinic, $C2/c$
a (Å)	61.5935(3)	61.1492(3)	60.8915(4)
b (Å)	15.6399(1)	15.5084(1)	15.4268(1)
c (Å)	17.9843(1)	17.7700(1)	17.6013(2)
α (deg)	90.0	90.0	90.0
β (deg)	95.8549(2)	95.6666(3)	95.3729(4)
γ (deg)	90.0	90.0	90.0
V (Å^3)	17234.19(17)	16769.41(16)	16461.3(2)
Z	8	8	8
D_{calc} (Mg/m^3)	1.478	1.476	1.582[a]
θ range (deg)	4.19−25.03	4.11−25.01	4.09−25.05
F(000)	7608	7608	7808
μ (mm^{-1})	0.866	0.890	0.909
data collection method	ω-2θ scans	ω-2θ scans	ω-2θ scans
collected/unique reflns	27 491/15 042	14 612/11 049	14 368/12 283
criterion for observed reflns	$I > 2\sigma(I)$	$I > 2\sigma(I)$	$I > 2\sigma(I)$
R_{int}	0.0253	0.0254	0.0254
ranges of h, k, l	$-73 \rightarrow h \rightarrow +73$	$-72 \rightarrow h \rightarrow +72$	$-72 \rightarrow h \rightarrow +72$
	$-18 \rightarrow k \rightarrow +17$	$-18 \rightarrow k \rightarrow +18$	$-18 \rightarrow k \rightarrow +18$
	$-21 \rightarrow l \rightarrow +21$	$-21 \rightarrow l \rightarrow +21$	$-20 \rightarrow l \rightarrow +20$
completeness to 2θ	0.986	0.988	0.985
reflns/restraints/param	15 042/0/1020	14 612/0/1084	14 368/0/1116
GOF on F^2	1.022	1.036	1.035
$\Delta\rho_{max}$, $\Delta\rho_{min}$ (e/Å^3)	1.193, −0.569	1.287, −0.696	1.054, −0.703
R1, wR2 [$I > 2\sigma(I)$]	0.0910, 0.2513	0.0721, 0.1915	0.0549, 0.1379
R1, wR2 (all)	0.1124, 0.2744	0.0966, 0.2097	0.0639, 0.1454

[a] Includes solvation molecules resolved at 100 K.

distant aminoxyl group of the **3PPN** unit; that spin polarization is virtually nil, based on our earlier work.[6] This presumably also applies to the other complexes.

General Comparisons. Kinetic and/or thermodynamic factors apparently favor **M2L2** loop formation incorporating the syn conformer of **3PPN** both in clusters and in extended solids. We obtained no analogous loop-incorporating, higher-dimensional solids with **4PPN**, despite repeated efforts.[3,4] Chain linking of M_2L_2 loops in a possible **Chain4PPN** may be unfavorable because it requires significant zigzag extension, as opposed to the near perfectly linear, trans geometry of cross-linking in **Chain** from **3PPN**-containing loops (Scheme 8).

The Cu−ON bonds in most of the complexes in this study shorten during spin-state conversion to AFM exchange as the temperature drops; a few are already AFM exchange-coupled at room temperature. The spin-state conversions are gradual as the temperature drops, even in extended coordination systems like **Net2anti** and **Net3d**. This differs from the relatively sharp spin-crossover (SCO) transitions seen in complexes that exhibit synergistic interaction between network coordination sites.[21]

The Cu−N bond lengths with pyrimidine nitrogen atoms vary significantly among the Table 1 complexes. In loops, they are consistently 2.0−2.1 Å long, where Cu^{II} coordinates only one pyridimidine at a time. They are more variable when two pyrimidines are coordinated to Cu^{II}, ranging from just under 2.0 Å to nearly 2.5 Å. None vary strongly with the temperature (<0.1 Å).

The variety of products obtained by the reaction of Cu(hfac)$_2$ with **3PPN** presented some challenges for isolation and characterization. However, complexation of copper(II) with radical ligands has produced even more challenging product variability in some other cases. Ovcharenko and co-workers reported[22] that the reaction of Cu(hfac)$_2$ with 4,4,5,5-tetramethyl-2-(1-methyl-1*H*-pyrazol-4-yl)imidazoline-3-oxide-1-oxyl (**MePyrNN**, Chart 2) yielded 12 distinct complexes, with varying magnetic behavior. Solvent incorporation was important in forming some of those phases, analogous to the role of hexane incorporation in **Net3d** in our work.

The Cu$_x$(**MePyrNN**)$_y$(hfac)$_{2x}$ family of complexes consists of clusters and 1D chains as far as bonded connectivity is concerned. Ovcharenko and co-workers carried out extensive studies while classifying these and similar coordination complexes as "breathing crystals",[23] which exhibit reversible coordination sphere and unit cell dimension changes with varying temperature. They note that such systems show promise for having electronically switchable behavior because of the temperature and even photochemical reversibility of high-temperature weak exchange coupling between inorganic and organic spin units (M···ON exchange) and strong low-temperature AFM exchange. The complexes in the present study have similar behavior in many respects and may have similar promise.

Ovcharenko and co-workers also pursued extension of the connective dimensionality of their complexes by using **MePyr-NN** biradical ligands composed of monoradicals connected by flexible linkers, **(MePyrNN)$_2$(CH$_2$)$_n$** with $n = 4$ and 8 (Chart 2). This approach successfully yielded 2D and 3D networks with macrocyclic and macrohelical secondary structure.[24] The polymethylene linkers in the biradical ligands in their work are the structural cross-links in the overall crystal lattice. In contrast, in our work paramagnetic Cu(hfac)$_2$ provides cross-links between radical ligands, giving more paramagnetic spins per radical unit with M_3L_2 stoichoimetry instead of $M_2L{-}L$ (where L−L are the linked radicals in Ovcharenko group's [**MePyrNN)$_2$(CH$_2$)$_{4,8}$** biradical ligands]. Although the **3PPN** radical ligand used in the present study is far more rigid than the L−L radicals in **(MePyrNN)$_2$(CH$_2$)$_n$**, the **3PPN** single-bond torsional flexibility is sufficient to form extended coordination networks of Cu(hfac)$_2$ because both linear and highly bent chain geometries are possible.

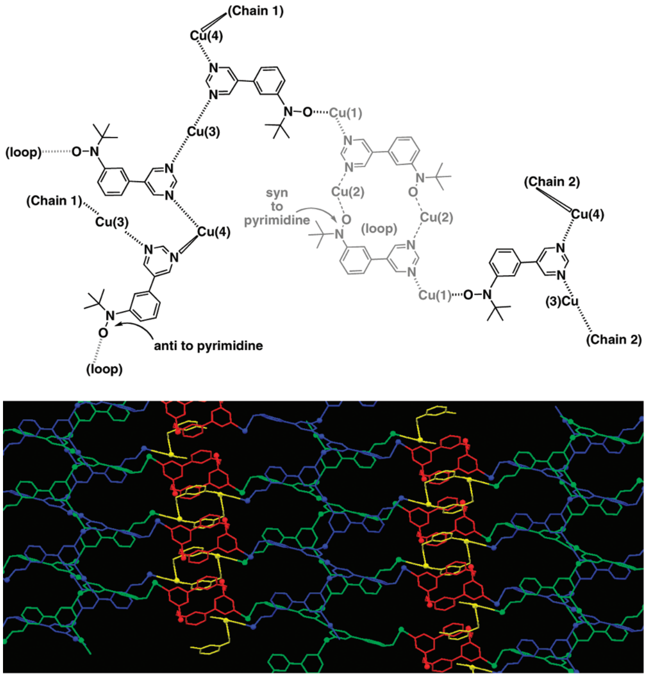

Figure 14. (Upper) Schematic of **Net3d** connectivity; chains 1 and 2 cross-link to other chains to give a 3D net. (Lower) Colorized in 3D to show different chains (blue and green) and loops (red and yellow), with omission of the hfac units.

CONCLUSIONS

Multiple extended dimensionality complexes form by reacting the hinge-flexible **3PPN** radical ligand with Cu(hfac)$_2$. Cyclic **M2L2** loops are favored both as isolated clusters and as parts of extended solids. No isolated **ML2** systems were isolated. Both helical and 1D chains form with connectivity (−Cu−Pyrim−Ph−NO−)$_n$, but only as part of 2D networks that also have Pyrim−Cu−Pyrim cross-links. A complex 3D network solid, **Net3d**, was composed of **M2L2** units cross-linked by −Cu−**3PPN**− chains. The **M2L2** loops and the 2D and 3D solids could be obtained in tens of milligram amounts; the **Chain** and **M3L4** complexes were only obtained in yields of a few milligrams, presumably as kinetic products.

The magnetic behavior of most of the complexes was dominated by reversible spin-state conversion of ferromagnetically or poorly exchange-coupled Cu−ON spin units to give antiferromagnetically coupled low-spin-state units at lower temperatures. All of the complexes exhibit conversion over fairly broad temperature ranges. **Net3d**, the only network with (−Cu−Pyrim−)$_n$ extended chain formation, also showed AFM exchange between Cu^{II} ions across pyrimidine units.

This study shows that allowing flexible "sharp-turn" geometries for coordination between paramagnetic metal ions and radical ligands assists the formation of loops and chains. As a general strategy, this offers a wide range of possibilities for making 2D and 3D network solids with unusual magnetic properties.

EXPERIMENTAL SECTION

General Procedures. Diethyl ether and tetrahydrofuran were distilled under argon from sodium. *N,N*-Dimethylformamide was dried over anhydrous magnesium sulfate. Silver(I) oxide was freshly made by treatment of silver(I) nitrate with sodium hydroxide, washing of the resultant precipitate with distilled water, and air drying. All melting points are uncorrected.

Variable-temperature magnetic susceptibility measurements were carried out on a Quantum Design MPMS-5 SQUID magnetometer at the Nanomagnetics Characterization Facility at UMass—Amherst. Samples were placed into gelatin capsules, held in place with a plug of cotton, and subjected to a helium atmosphere purge before measurement. Paramagnetic susceptibilities were determined by subtraction of temperature-independent magnetic contributions from the raw data.

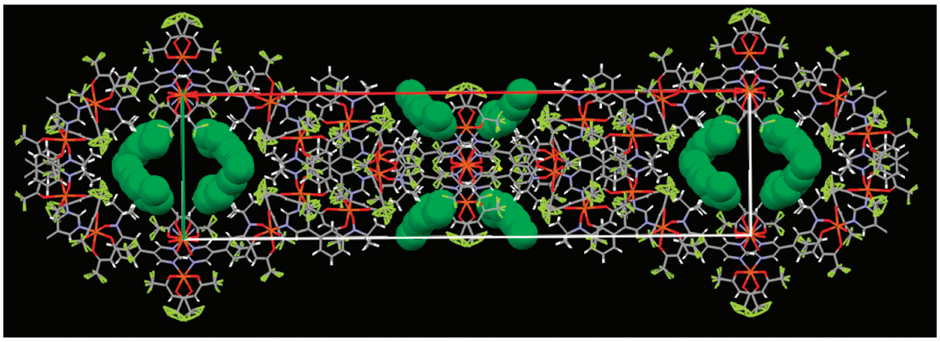

Figure 15. Hexane of solvation (green space-filling) in the void space of the **Net3d** lattice, from a 100 K crystal structure, viewed down the *c* axis in the *ab* plane.

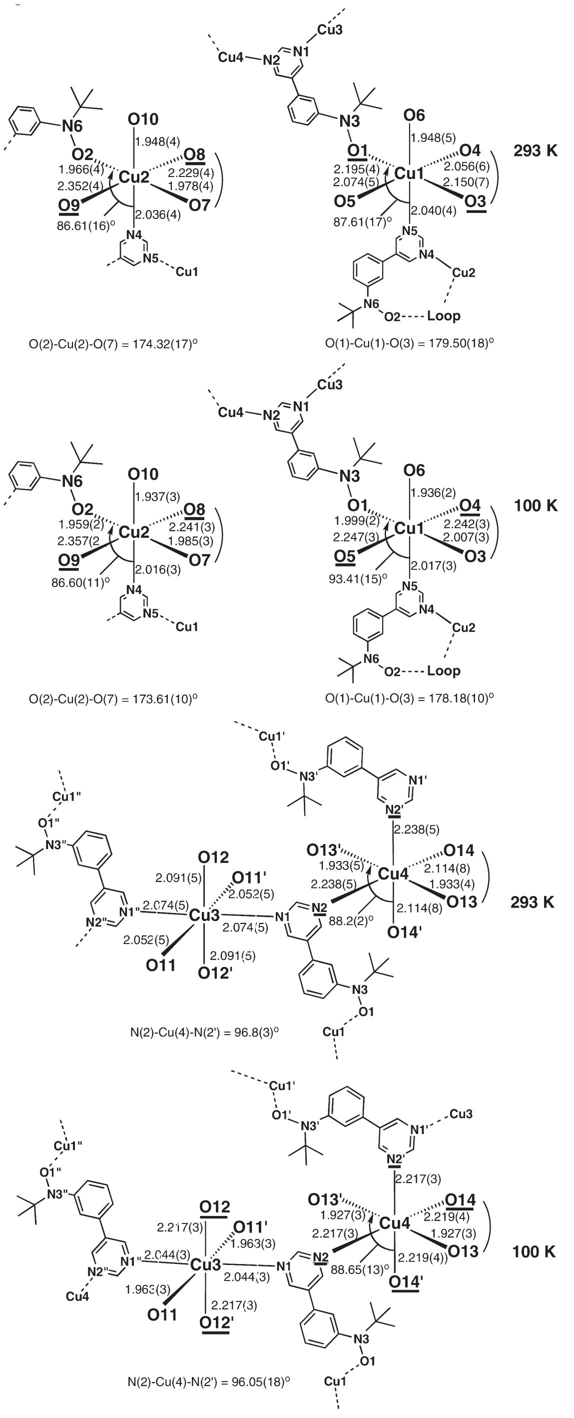

Figure 16. Ligand-sphere changes with the temperature for the different copper(II) environments in **Net3d**. Bond lengths are in angstroms and angles in degrees. Long bond ligated atoms are underlined.

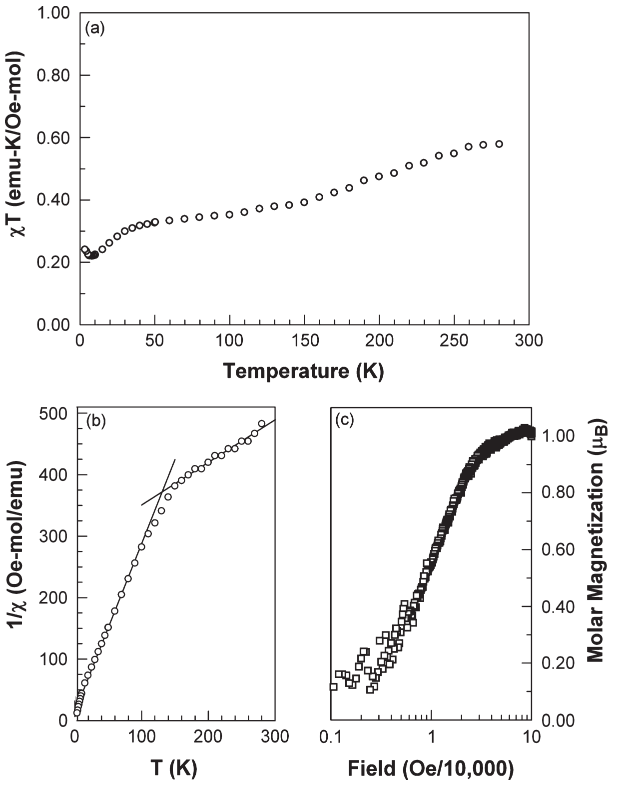

Figure 17. For **Net3d**, (a) χT data vs T and (b) $1/\chi$ vs T both at 500 Oe external field and (c) magnetization versus field at 1.4 K. The solid lines in plot b are Curie–Weiss fits to data <100 and >150 K.

Scheme 7. Proposed Mechanism of Cross-Ring Pyrimidine-Mediated AFM Exchange between Cu^{II} Ions in the Chains of Net3d

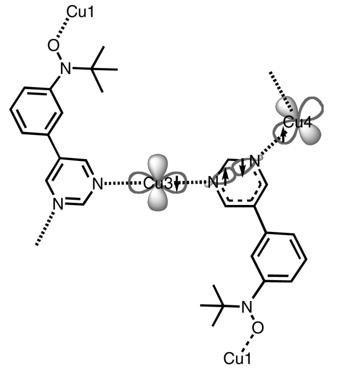

Molar magnetization versus field experiments (M vs H) were carried out using a custom-built apparatus[25] at Universidade de São Paulo.

Elemental analyses were carried out by Dr. G. Dabkowski of the UMass—Amherst Microanalysis Laboratory. High-resolution mass spectra were obtained by Dr. Stephen Eyles of the UMass—Amherst Mass Spectrometry and Molecular Weight Facility.

Preparation of 5-[3-(*N*-*tert*-Butyl-*N*-aminoxyl)phenyl]pyrimidine (3PPN). Compound **3PPNH** was made as described previously.[6] Silver(I) oxide (0.531 g, 2.29 mmol) was then added to a stirred solution of **3PPNH** (0.223 g, 0.917 mmol) in benzene (20 mL) under argon. After 2 h, the reaction was filtered to yield a clear red/orange solution. This can be used directly for spectroscopic studies and as a reactant in subsequent reactions. The radical can be isolated as an oil by solvent removal without heating; it is not stable to prolonged storage and so is best used as soon as possible after preparation. Electron pramagnetic resonance (benzene, room temperature, 9.649 GHz): a_N = 12.28 G, a_H = 2.03, 1.92, 1.82, 0.83 G.

Cu$_3$(3PPN)$_4$(hfac)$_6$ (M3L4). **3PPNH** (0.060 g, 0.247 mmol) in 2 mL of dichloromethane under argon was stirred over silver(I) oxide (0.114 g, 0.493 mmol) to give a solution of radical **3PPN** and then was filtered through Celite. Cu(hfac)$_2\cdot x$H$_2$O (0.122 g, 0.247 mmol) was dissolved in a

Scheme 8. “Chaining” of M_2L_2 Loops in 3PPN by Linear Extension, Compared to 4PPN

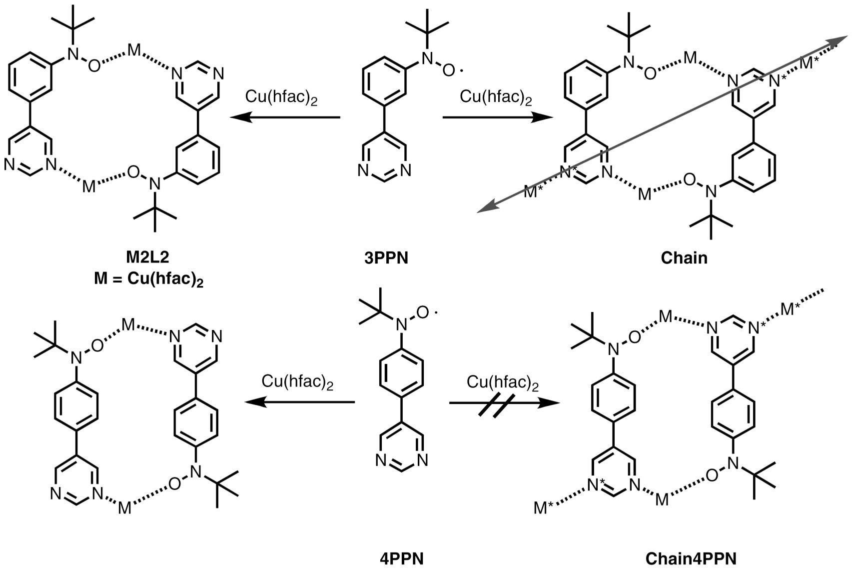

Chart 2

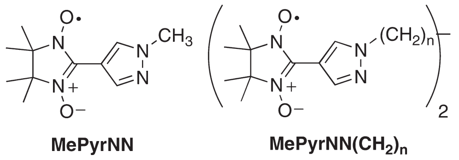

solution of 0.5 mL of diethyl ether and 1 mL of dichloromethane. The **3PPN** solution was layered atop the Cu(hfac)$_2$ solution and then covered with a layer of distilled hexanes. After 4 days, a mixture of green and yellow crystals precipitated; a few milligrams of the green crystals were separated manually. Single-crystal XRD analysis was carried out. The crystal and structural parameters in CIF format were deposited at the Cambridge Crystallographic Data Centre as CCDC.

$Cu_2(3PPN)_2(hfac)_4$ (M2L2). The complex was synthesized as previously described[6] to give a brownish powder (which reversibly turns green upon cooling in liquid nitrogen), which yields yellow-green needles when recrystallized by slow evaporation from toluene. Mp: 104−106 °C. The crystal and structural parameters in CIF format have been deposited at the Cambridge Crystallographic Data Centre (PAXBAS, PAXBAS02).

$Cu_3(3PPN)_2(hfac)_6$ (Chain). Compound **3PPNH** (7 mg, 0.03 mmol) was oxidized in benzene by the procedure described above, filtered, and evaporated, and the resulting **3PPN** was dissolved in dichloromethane (0.1 mL) in a 5 mL test tube. Cu(hfac)$_2 \cdot x H_2O$ (3 mg, 7.0 micromol) was dissolved in a mixture of dichloromethane (0.2 mL) and hexanes (1.0 mL), which was carefully layered atop the red radical solution. After 4 days, green and yellow crystals appeared in the test tube. The green crystals were manually separated for analysis and single-crystal XRD work. The crystal and structural parameters in CIF format were deposited at the Cambridge Crystallographic Data Centre as CCDC.

$Cu_3(3PPN)_2(hfac)_6$ (Net2syn). **3PPNH** (0.223 g, 0.917 mmol) was oxidized as described above, filtered, and evaporated, and the product **3PPN** was dissolved in dichloromethane (6.5 mL) and pipetted into a 25 mL graduated cylinder. Cu(hfac)$_2 \cdot x H_2O$ (0.454 g, 0.917 mmol) was dissolved in dichloromethane (6.0 mL) and hexanes (14.0 mL) and layered on top of the radical solution. Crystals formed after 1 week. Mp: 114−119 °C. Single-crystal XRD analysis was carried out. The crystal and structural parameters in CIF format were deposited at the Cambridge Crystallographic Data Centre.

$Cu_3(3PPN)_2(hfac)_6$ (Net2anti). Compound **3PPNH** (0.060 g, 0.247 mmol) was stirred for 2 h over silver(I) oxide (0.114 g, 0.493 mmol) in dichloromethane (1.5 mL) under argon to give a red solution of **3PPN**, which was filtered through Celite into a glass vial. Cu(hfac)$_2 \cdot x H_2O$ (0.122 g, 0.247 mmol) was dissolved in a mixture of distilled diethyl ether (2.0 mL), dichloromethane (2.0 mL), and distilled hexanes (5.0 mL), which was then carefully layered atop the **3PPN** solution: then 5.0 mL of distilled hexanes was layered on top of this. Crystals formed after 5 days. Mp: 107−108.5 °C. Single-crystal XRD analysis was carried out. The final parameters in CIF format were deposited at the Cambridge Crystallographic Data Centre as CCDC.

$Cu_3(3PPN)_2(hfac)_6$ (Net3d). Compound **3PPNH** (0.153 g, 0.627 mmol) was stirred with silver(I) oxide (0.182 g, 0.784 mmol) in dichloromethane (2 mL) under argon to give a red solution of **3PPN**, which was filtered through Celite into a 5 mL test tube. Cu(hfac)$_2 \cdot x H_2O$ (0.466 g, 0.941 mmol) was dissolved in a mixture of dichloromethane (1 mL), diethyl ether (1 mL), and distilled hexane (5 mL), which was carefully layered atop the solution of **3PPN**. After 5 days, large dark-green-yellow crystals formed. Mp: 123.5−124.5 °C. Single-crystal XRD analysis was carried out. The crystal and structural parameters in CIF format were deposited at the Cambridge Crystallographic Data Centre as CCDC.

■ ASSOCIATED CONTENT

Ⓢ Supporting Information. General synthetic procedures, ORTEP diagrams, and CIF format crystallographic summaries for all complexes and for **3PPNH**, chain packing diagrams for **Chain**, **Net2syn**, and **Net2anti**, 100 K crystallographic analysis procedure for **Net2anti** and a comparison to the structure at room temperature, diagrams of void space solvation in **Net3d**, and powder XRD for **Net2syn** compared to simulations from other single-crystal XRD. This material is available free of charge via the Internet at http://pubs.acs.org.

AUTHOR INFORMATION

Corresponding Author

*E-mail: lahti@chem.umass.edu.

ACKNOWLEDGMENT

M.B. and P.M.L. thank the U.S. National Science Foundation for support through Grants CHE-0109094 and CHE-0415716. A.P.-F. and N.F.O. thank Fundação de Amparo à Pesquisa do Estado de São Paulo (FAPESP) in Brazil for support. J.T.M. thanks the Louisiana Board of Regents through the Louisiana Educational Quality Support Fund (Grant 2003-ENH-TR-67) for the purchase of a diffractometer and the Tulane University Chemistry Department for support of the X-ray diffraction facility.

REFERENCES

(1) (a) Kahn, O. *Molecular Magnetism*; VCH: New York, 1993. (b) Iwamura, H.; Inoue, K.; Hayamizu, T. *Pure Appl. Chem.* **1996**, *68*, 243. (c) Caneschi, A.; Gatteschi, D.; Sessoli, R.; Rey, P. *Acc. Chem. Res.* **1989**, *22*, 392.(d) Caneschi, A.; Gatteschi, D.; Sessoli, R. In *Magnetic Molecular Materials*; Gatteschi, D., Kahn, O., Miller, J. S., Palacio, F., Eds.; Kluwer: Dordrecht, The Netherlands, 1991; p 215. (e) Gatteschi, D.; Rey, P. In *Magnetic Properties of Organic Materials*; Lahti, P. M., Ed.; Marcel Dekker: New York, 1999. (f) Caneschi, A.; Gatteschi, D.; Rey, P. In *Progress in Inorganic Chemistry*; Lippard, S. J., Ed.; Wiley: New York, 1991; Vol. 39, p 331. (g) Ouahab, L. *Coord. Chem. Rev.* **1998**, *178−180*, 1501. (h) Hicks, R. G. *Aust. J. Chem.* **2001**, *54*, 597. (i) Lemaire, M. T. *Pure Appl. Chem.* **2004**, *76*, 277.

(2) Field, L. M.; Lahti, P. M.; Palacio, F.; Paduan-Filho, A. *J. Am. Chem. Soc.* **2003**, *125*, 10110.

(3) Field, L. M.; Lahti, P. M. *Inorg. Chem.* **2003**, *42*, 7447.

(4) Lahti, P. M.; Baskett, M.; Field, L. M.; Morón, M. C.; Palacio, F.; Paduan-Filho, A.; Oliveira, N. F., Jr. *Inorg. Chim. Acta* **2008**, *361*, 3697–3709.

(5) Field, L. M.; Morón, M. C.; Lahti, P. M.; Palacio, F.; Paduan-Filho, A.; Oliveira, N. F., Jr. *Inorg. Chem.* **2006**, *45*, 2562.

(6) Baskett, M.; Lahti, P. M.; Paduan-Filho, A.; Oliveira, N. F., Jr. *Inorg. Chem.* **2005**, *44*, 6725.

(7) Field, L. M.; Lahti, P. M. *Polyhedron* **2005**, *24*, 2639.

(8) Ishimura, Y.; Inoue, K.; Koga, N.; Iwamura, H. *Chem. Lett.* **1994**, 1693.

(9) Ishimaru, Y.; Kitano, M.; Kumada, H.; Koga, N.; Iwamura, H. *Inorg. Chem.* **1998**, *37*, 2273.

(10) (a) Kitano, M.; Ishimaru, Y.; Inoue, K.; Koga, N.; Iwamura, H. *Inorg. Chem.* **1994**, *33*, 6012. (b) Rabu, P.; Drillon, M.; Iwamura, H.; Gorlitz, G.; Itoh, T.; Matsuda, K.; Koga, N.; Inoue, K. *Eur. J. Inorg. Chem.* **2000**, 211.

(11) See also a summary in: Iwamura, H.; Koga, N. *Mol. Cryst. Liq. Cryst.* **1999**, *334*, 437.

(12) Yamada, K.; Yagishita, S.; Tanaka, H.; Tohyama, K.; Adachi, K.; Kaizaki, S.; Kumagai, H.; Inoue, K.; Kitaura, R.; Chang, H.-C.; Kitagawa, S.; Kawata, S. *Chemistry* **2004**, *10*, 2647.

(13) Software for crystallographic pictures includes the following. (a) *Mercury*, version 2.4, Cambridge Crystallographic Data Centre: Macrae, C. F.; Bruno, I. J.; Chisholm, J. A.; Edgington, P. R.; McCabe, P.; Pidcock, E.; Rodriguez-Monge, L.; Taylor, R.; van de Streek, J.; Wood, P. A. *J. Appl. Crystallogr.* **2008**, *41*, 466–470. (b) ORTEP-3 for Windows: Farrugia, L. J. *J. Appl. Crystallogr.* **1997**, *30*, 565.

(14) (a) Caneschi, A.; Gatteschi, D.; Sessoli, R.; Rey, P. *Acc. Chem. Res.* **1989**, *22*, 392.(b) Caneschi, A.; Gatteschi, D.; Sessoli, R. In *Magnetic Molecular Materials*; Gatteschi, D., Kahn, O., Miller, J. S., Palacio, F., Eds.; Kluwer: Dordrecht, Netherlands, 1991; p 215. (c) Gatteschi, D.; Rey, P. In *Magnetic Properties of Organic Materials*; Lahti, P. M., Ed.; Marcel Dekker: New York, 1999.

(15) See a similar case in: Lanfranc de Panthou, F.; Belorizky, E.; Calemczuk, R.; Luneau, D.; Marcenat, C.; Ressouche, E.; Turek, P.; Rey, P. *J. Am. Chem. Soc.* **1995**, *117*, 11247.

(16) (a) Luneau, D.; Rey, P.; Laugier, J.; Fries, P.; Caneschi, A.; Gatteschi, D.; Sessoli, R. *J. Am. Chem. Soc.* **1991**, *113*, 124. (b) Ressouche, E.; Boucherle, J.-X.; Gillon, B.; Rey, P.; Schweizer, J. J. *J. Am. Chem. Soc.* **1993**, *115*, 3610. (c) Boucherle, J.-X.; Ressouche, E.; Schweizer, J.; Gillon, B.; Rey, P. *Z. Naturforsch.* **1993**, *48*, 120.

(17) (a) Choe, W.; Pecharsky, V. K.; Pecharsky, A. O.; Gschneider, K. A.; Young, V. G., Jr.; Miller, G. J. *Phys. Rev. Lett.* **2000**, *84*, 4717. (b) Colombo, D. G.; Young, V. G., Jr.; Gladfelter, W. L. *Inorg. Chem.* **2001**, *39*, 4621. (c) Jazdzewski, B. A.; Holland, P. L.; Pink, M.; Young, V. G., Jr.; Spencer, D. J. E.; Tolman, W. B. *Inorg. Chem.* **2001**, *40*, 6097.

(18) (a) Borden, W. T., Ed. *Diradicals*; Wiley: New York, 1982. (b) Borden, W. T.; Iwamura, H.; Berson, J. A. *Acc. Chem. Res.* **1994**, *27*, 109. (c) Fang, S.; Lee, M.-S.; Hrovat, D.; Borden, W. T. *J. Am. Chem. Soc.* **1995**, *117*, 6727.

(19) Glaser, T.; Lügger, T.; Fröhlich, R. *Eur. J. Inorg. Chem.* **2004**, 394 and references cited therein.

(20) Mohri, F.; Yoshizawa, K.; Yamabe, T.; Ishida, T.; Nogami, T. *Mol. Eng.* **1999**, *8*, 357.

(21) (a) Gütlich, P.; Garcia, Y.; Goodwin, H. A. *Chem. Soc. Rev.* **2000**, *29*, 419. (b) Niel, V.; Thompson, A. L.; Muñoz, M. C.; Galet, A.; Goeta, A. E.; Real, J. A. *Angew. Chem., Int. Ed.* **2003**, *42*, 3760. (c) Bousseksou, A.; Molnar, G.; Matouzenko, G. *Eur. J. Inorg. Chem.* **2004**, *22*, 4353.(d) Gütlich, P., Goodwin, H. A., Eds. *Topics in Current Chemistry*; Springer: Berlin, 2004; Vols. 232−234.

(22) Fokin, S.; Ovcharenko, V.; Romanenko, G.; Ikorskii, V. *Inorg. Chem.* **2004**, *43*, 969.

(23) (a) Ovcharenko, V. In *Stable Radicals: Fundamentals and Applied Aspects of Odd-Electron Compounds*; Hicks, R. G., Ed.; John Wiley & Sons, Ltd.: Chichester, U.K., 2010; Chapter 13. (b) Fedin, M. V.; Veber, S. L.; Maryunina, K. Yu.; Romanenko, G. V.; Suturina, E. A.; Nina, P.; Gritsan, N. P.; Sagdeev, R. Z.; Ovcharenko, V. I.; Bagryanskaya, E. G. *J. Am. Chem. Soc.* **2010**, *132*, 13886. (c) Veber, S. L.; Fedin, M. V.; Maryunina, K. Yu.; Romanenko, G. V.; Renad, Z.; Sagdeev, R. Z. *Inorg. Chim. Acta* **2008**, *361*, 4148. (d) Fedin, M. V.; Veber, S. L.; Romanenko, G. V.; Ovcharenko, V. I.; Sagdeev, R. Z.; Klihm, G.; Reijerse, E.; Lubitz, W.; Bagryanskaya, E. G. *Phys. Chem. Chem. Phys.* **2009**, *11*, 6654. (e) Fedin, M.; Ovcharenko, V.; Sagdeev, R.; Reijerse, E.; Lubitz, W.; Bagryanskaya, E. *Angew. Chem., Int. Ed.* **2008**, *47*, 6897.

(24) Treyakov, E.; Fokin, S.; Romanenko, G.; Ikorskii, V.; Vasilevsky, S.; Ovcharenko, V. *Inorg. Chem.* **2006**, *45*, 3671.

(25) Oliveira, N. F., Jr.; Paduan-Filho, A.; Salinas, S. R.; Becerra, C. C. *Phys. Rev. B* **1978**, *18*, 6165.